

A Preprocessing Approach for Innovative Patient-specific Intranasal Flow Simulations

Mathias J. Krause^{1*}, Thomas Gengenbach¹, Rolf Mayer², Simon Zimny¹,
Vincent Heuveline¹

¹Engineering Mathematics and Computing Lab (EMCL), Karlsruhe Institute of
Technology (KIT), Fritz-Erler-Str. 23, 76133 Karlsruhe, Germany

²Steinbuch Centre for Computing (SCC), Karlsruhe Institute of Technology (KIT),
Zirkel 2, 76131 Karlsruhe, Germany

Abstract. A preprocessing approach which enables numerical simulations of patient-individual respiration flows based on computer tomography (CT) scans is presented. The challenge of an adequate 3D reconstruction and preparation of as highly complex geometries as the human inner nose or lung, which cannot be resolved in all their details by nowadays available CT scanners, is met by a holistic concept. In it, the preprocessing is understood as one part of the *full numerical simulation* where preprocessing, numerical simulation and optimization as well as postprocessing techniques are applied in an iteratively coupled fashion. In the proposed approach, lattice Boltzmann methods are chosen as discretization strategy in order to simulate the airflows. Since they impose the conditions for the preparation process of the geometries, this choice is of crucial importance for the preprocessing techniques which are to be applied. For the actual preprocessing steps, it is proposed to take advantage of techniques, which are implemented in the framework of Materialise's software packages Mimics and 3-matics. In this paper, main emphasis is placed on illustrating the preprocessing approach as part of the proposed full numerical simulation concept. Therefore, the whole chain of necessary processes from the segmentation over the surface generation, the actual volume mesh generation, the numerical simulation, the validation up to the visualization of the results is demonstrated by means of an example, namely the full numerical simulation of an expiration in an inner human nose. The researched geometry belongs to a patient with a severe peripheral obstructive ventilation disorder. Based on the obtained numerical results, possible causes and consequences are discussed, in particular, a stenosis is located.

Keywords: preprocessing, numerical patient-specific fluid flow simulation, lattice Boltzmann methods, human respiratory system, nasal cavity, otolaryngology

* Correspondence to: mathias.krause@kit.edu

1 Introduction

For almost all humans a rough rule of thumb holds:

3 weeks without food, 3 days without water and 3 minutes without air.

This so-called “Rule of Three” first came up in different survival handbooks, but shows impressively the most important need of humans, which is oxygen. Hence in the last century, different research projects arose, aiming at simulating airflows either in the human nose or in the upper generations of the human lung.

Respiratory illnesses are the second most frequent diseases with respect to mortality, incidence, prevalence and the cost for the health care system [50]. Due to the research in this area, it is by now possible to detect the symptoms arising from illnesses of the human respiratory tract, but still, very little is known about the actual cause of these symptoms. Modeling, numerical simulations and optimization can help to gain a deeper insight in the functionality of the airways. Hence they enable achieving a better knowledge of the respiratory system and the factors that cause diseases.

Driven by the rapid increase of available computing power in recent years, especially in the context of *high performance computing* (HPC), the relevance of *computational fluid dynamics* (CFD) for medical research and development in this area has grown steadily. With the adaption of efficient numerical methods to parallel computing platforms it is possible to tackle problems that arise in everyday clinical situations. For example, the simulation of intranasal flows based on *computer tomography* (CT) data help physicians to plan surgeries and, moreover, quantify the possible benefit of a surgery beforehand. This is especially important for patients with a deviated septum. Another application constitutes the optimization and control of the dose rate of asthma sprays by means of numerical simulation. About 300 million people worldwide suffer from asthma and need to use asthma sprays in their daily routine [17]. The effectiveness of inhalers for asthmatics can be improved systematically e.g. by drug-aerosol targeting via optimizing the shape of the spray nozzles or the particle size of an aerosol.

Before a numerical simulation can be started, a representation of the discrete geometry together with the corresponding values for the initial and boundary conditions need to be provided. The required data must meet precise requirements which strongly depend on the considered numerical method. Images of the respiratory tract obtained by CT and certain measurements constitute the starting basis. However, parts of the geometry of the human nose are on such a small scale that they cannot be captured by the latest imaging techniques. Therefore, adequate *preprocessing* techniques need to be developed and applied to enable realistic numerical simulations of physical phenomena. Furthermore, the data for a numerical simulation may have to be prepared many times, e.g. for patient-individual flow simulations in the daily hospital’s routine or for technical reasons. In this context adaptive techniques are to be mentioned since they require a coupling of preprocessing, simulation and optimization techniques (cf. e.g. [14] and references therein). In this framework, *a posteriori error estimation methods* [5] are employed together with grid refinement strategies to obtain

more accurate results. These examples clearly show that the preprocessing cannot be considered as independent process. In fact, the preprocessing is rather a part of the *full numerical simulation* which also comprises the actual numerical simulation, possible optimization as well as the postprocessing. In Figure 1 the relations of the single elements of the full numerical simulation are depicted schematically.

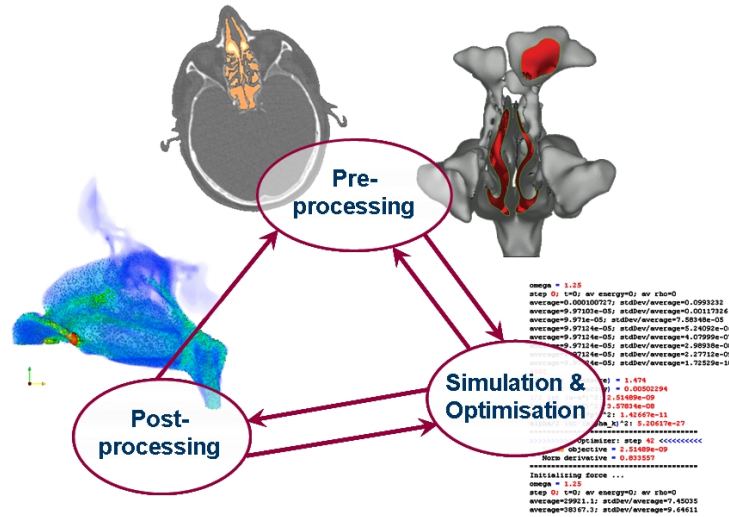


Fig. 1: Cycle of full numerical simulation exemplified for the simulation of the airflow in a human nose. The importance of the preprocessing as one part of a full numerical simulation concept becomes obvious and, consequently, the imperative to automate preprocessing steps.

As a consequence of the prominent role of the preprocessing in the framework of the full numerical simulation, the requirement for a high level of automatization of preprocessing steps reveals. This need is strengthened by the fact that the complexity of the geometry makes handiwork to an exhausting and hence almost impossible task.

In this paper, a concept for a complete preprocessing approach, dedicated to simulate the highly complex flow in the human nose, is presented. Thereby, emphasis is placed on obtaining a preferably automatized approach. The overall strategy consists of three main steps which build up the following chain:

$$\text{CT data} \xrightarrow{\text{Sec. 3}} \text{Surface mesh} \xrightarrow{\text{Sec. 4}} \text{Volume mesh} \xrightarrow{\text{Sec. 5}} \text{Simulation} .$$

A separate section is devoted to describe each of these steps. There, the concept is explained by considering the preprocessing of a flow simulation in a

human nasal cavity. All preprocessing steps are illustrated by a series of images in the Figures 6 to 9, showing the segmented CT data, the surface mesh, the volume mesh and finally the obtained numerical results at six particular chosen slices of the nasal cavity.

Due to the embedding of the preprocessing in the cycle of full numerical simulation, the choice of the numerical method to solve the fluid flow problem is crucial for the design of the preprocessing approach and, consequently, for its success. Here, *lattice Boltzmann Methods* (LBM) are chosen. They have become a mature technique in the context of CFD in the last two decades (cf. literature e.g. [11,22,52]) and have shown to be very attractive for computationally highly expensive simulations as well as for simulations with complex underlying computational domains [34]. Hence, they are particularly well suited for the simulation of airflows in the human respiratory system. In front of the main part about the preprocessing approach, Section 3 to 5, Section 2 is placed which is dedicated to introduce the LB discretization strategy.

Finally, in the last section of this paper, numerical simulation results are presented in the context of a case study of an intranasal flow simulation. The study illustrates the applicability of the preprocessing approach and additionally demonstrates the great social impact and economic potential of patient-specific full numerical simulations which comprise an automated preprocessing.

The work which is presented here has been done in the framework of two projects, namely *United Airways* and *OpenLB*. A short overview of both projects is given in Appendix A and Appendix B.

2 Lattice Boltzmann Methods

A lattice Boltzmann (LB) numerical model simulates the dynamics of particle distribution functions $f = f(t, \mathbf{r}, \mathbf{v})$ in a phase space $\Omega \times \mathbb{R}^d$ with position $\mathbf{r} \in \Omega$ and velocity $\mathbf{v} \in \mathbb{R}^d$. The continuous transient phase space is replaced by a discrete space with a spacing of $\delta r = h$ for the positions, a set of $q \in \mathbb{N}$ vectors $\mathbf{v}_i \sim h^{-1}$ for the velocities and a spacing of $\delta t = h^2$ for time. The resulting discrete phase space is called the lattice and is labeled with the term $DdQq$. To reflect the discretization of the velocity space, the continuous distribution function f is replaced by a set of q distribution functions f_i ($q = 0, 1, \dots, q - 1$), representing an average value of f in the vicinity of the velocity \mathbf{v}_i . An exhaustive derivation of various LB equations can be found in the literature, e.g. in [52,11,22].

The iterative process in an LB algorithm can be written in two steps as follows, the collision step (1) and the streaming step (2):

$$\tilde{f}_i(t, \mathbf{r}) = f_i(t, \mathbf{r}) - \frac{1}{3\nu + 1/2} \left(f_i(t, \mathbf{r}) - M_{f_i}^{eq}(t, \mathbf{r}) \right), \quad (1)$$

$$f_i(t + h^2, \mathbf{r} + h^2 \mathbf{v}_i) = \tilde{f}_i(t, \mathbf{r}) \quad (2)$$

for $i = 0, 1, \dots, q - 1$, where

$$M_{f_i}^{eq}(t, \mathbf{r}) := \frac{w_i}{w} \rho_{f_i} \left(1 + 3h^2 \mathbf{v}_i \cdot \mathbf{u}_{f_i} - \frac{3}{2} h^2 \mathbf{u}_{f_i}^2 + \frac{9}{2} h^4 (\mathbf{v}_i \cdot \mathbf{u}_{f_i})^2 \right)$$

is a discretized Maxwell distribution with moments ρ and \mathbf{u} which are given according to

$$\rho := \sum_{i=0}^{q-1} f_i \quad \text{and} \quad \rho \mathbf{u} := \sum_{i=0}^{q-1} \mathbf{v}_i f_i .$$

The variable \mathbf{u} corresponds to the macroscopic fluid velocity and ρ to the mass density. The kinematic fluid viscosity is ν which is assumed to be given, and the terms w_i/w , $\mathbf{v}_i h$ ($i = 0, 1, \dots, q - 1$) are model dependent constants.

LBM, like the ones presented, are discretization strategies for families of BGK-Boltzmann equations (cf. [33]) which are related to a Navier-Stokes equation as shown by Saint-Raymond in [44]. Junk and Klar [30] interpret particular LB schemes of the presented type directly as Chorin-type projection methods for solving problems governed by an incompressible Navier-Stokes equation.

3 From CT Data to Surface Mesh

Computer tomography (CT) and *magnetic resonance imaging* (MRI) are standard image processing methods which are often applied in the area of medicine. A common standard file format for storing images, obtained by CT or MRI scanners, is the *digital imaging and communications in medicine* (DICOM) standard [40]. The data used hereafter is obtained by a CT scan with a SOMATOM Sensation 64 [47] and provided as DICOM files. In Figure 2 some images of the raw CT data are displayed. Different levels of gray scales reflect different material densities.

The mean resolution of the scans according to [47] is 0.4 mm. Even with this high resolution it is not possible to resolve all parts of the investigated human nose. Additionally, minor movements of the patient and electronic noise impede to obtain clear shapes of boundaries. In order to extract the volume of the nasal cavity which is filled with air, an *image segmentation technique* has to be applied. An overview of such approaches is given e.g. by Haralick et al. in [23]. Among that great variety of methods offered one finds *seeded* [4] and *dynamic region growing schemes* [48]. These enable robust and partly automated segmentation of a region which can be identified by its color level given by thresholds. Similar methods are implemented for example in the software package *Mimics* [42] from *Materialise NV* which is employed for the considered cases. In Figure 2 the complete segmented area of the CT data, that is connected and filled with air, is shown. The region comprises the inner nose and the area around the face outside the human body. In the Figures 6 and 8 the segmented CT data of chosen slices are depicted for the inner part of the human nose.

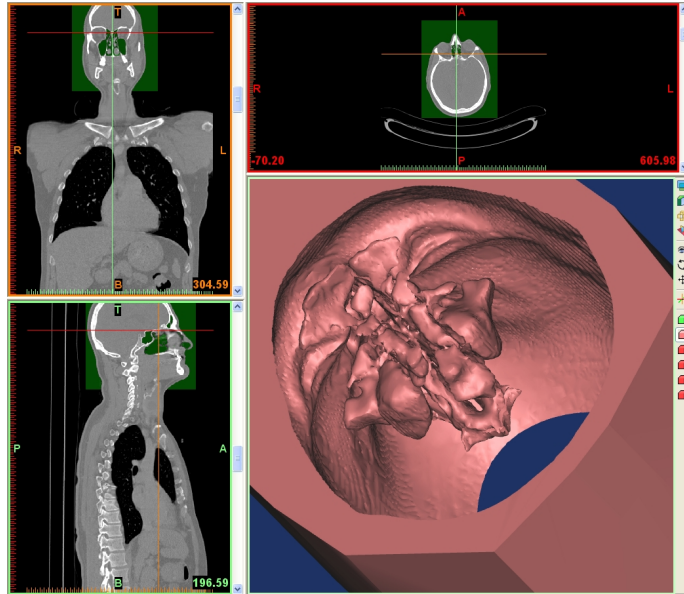


Fig. 2: The area of the CT data which is connected and filled with air, i.e. the inner nose and the area around the face outside the human body, is shown after the segmentation with *Mimics* [42] from *Materialise NV*.

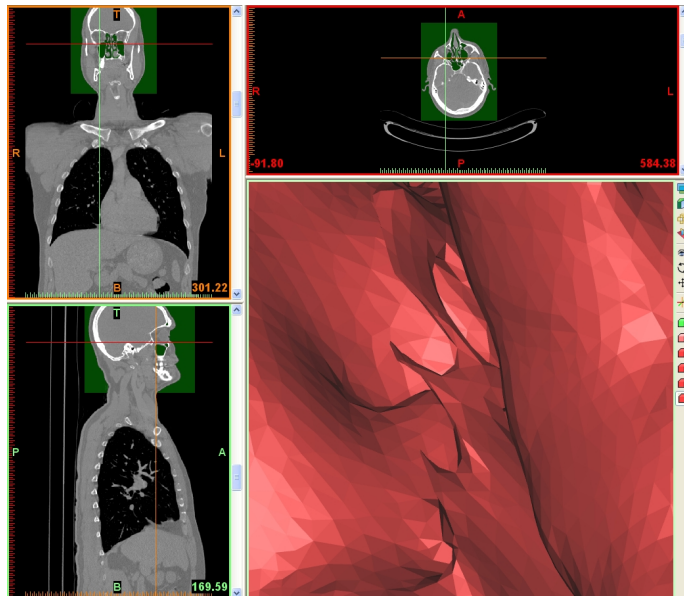


Fig. 3: A small tissue which separates two passages in the human inner nose could not be reconstructed completely from the CT data. The captured part forms a needle structure in the surface representation.

After the region of interest, here the inner human nose, has been segmented from the CT images the corresponding boundaries are to be extracted. This step is also performed with the help of the software package *Mimics*. As mentioned before, due to the limitation of nowadays available CT/MRT data scanner, the inner human nose cannot be captured in all its details, comprising many small air cavities like paranasal sinuses, thin passages and thin tissues. Yet, even these small incorrectly or not at all reconstructed parts can be relevant to the air-flow structure in the complete nasal cavity. Thus, an inadequate representation could lead to wrong numerical simulation results. As a consequence, a reconstruction of at least the relevant small structures is necessary. This work is done with the help of a physician and another software package of *Materialise NV*, namely *3-matic* [42], in an iterative process. For example, a small tissue which separates two passages could not be reconstructed completely. The captured part forms a needle structure in the surface representation (cf. Figure 3). The problem is solved by partly automated tools offered in the framework of *3-matic*. To get better insights of the inner nose's geometry, the surface is visualized in 3D at the *Lifecycle Engineering Solutions Center* (LESC) at the KIT, which provides a large stationary projection screen for immersive visualization with a high resolution. Tracking devices are used to navigate through the nose in a way as natural as possible and make sure that the geometry is correct. The geometry is interactively cut in every orientation, interactive markers are set at the surface locations and snapshots are taken where problems are identified.



Fig. 4: 3D visualization at LESC helps to get a more realistic surface representation of the nasal cavity.

Afterwards, the surface is smoothed and later approximated by a certain number of triangles. With this procedure an arbitrary fine resolution of the volume mesh can be obtained. The quasi file format standard *STL*, which is native to the stereolithography computer-aided design (CAD) software created by 3D Systems [3], serves as data format for the surface mesh. Figure 5 shows the inner and the outer part of the nose after the smoothing. The pictures in the Figures 6 and 8 visualize the geometry of the nasal cavity in the same chosen planes as before for the segmented CT data. The volume of this model is found to have a capacity of approximately 111.2 ml. 258,186 triangles are used to represent the surface which covers an area of about 469 cm².

4 From Surface Mesh to Volume Mesh

In order to solve fluid flow problems in the inner human nose numerically the continuous domain $\Omega \in \mathbb{R}^3$, which is given in terms of its boundary Γ as an STL surface representation of the nose, needs to be discretized. Standard LBM

require a uniform mesh $\Omega_h \cup \Gamma_h$ as discrete position space with discretization parameter $h \in \mathbb{R}_{>0}$ which is called the lattice.

A lattice can also be interpreted geometrically: each $r \in \Omega_h \cup \Gamma_h$ is seen as the center of a hexahedron with a length, height and depth of h . The hexahedrons are cubes which are in the following referred to as *voxels*. Consequently, a lattice is also said to be a *voxel mesh*. There exist a variety of techniques that enable obtaining such meshes for a given surface mesh and for arbitrary $h \in \mathbb{R}_{>0}$. Among there are methods known as *ray tracing*, *ray stabbing* or *parity count*. The latter two are proposed by Nooruddin et al. in [41]. They are implemented e.g. in the framework of the *Common Versatile Multi-purpose Library for C++* (CVMLCPP) which is an open source software invented by Beekhof [9] or the commercial software *HyperMesh* [6].

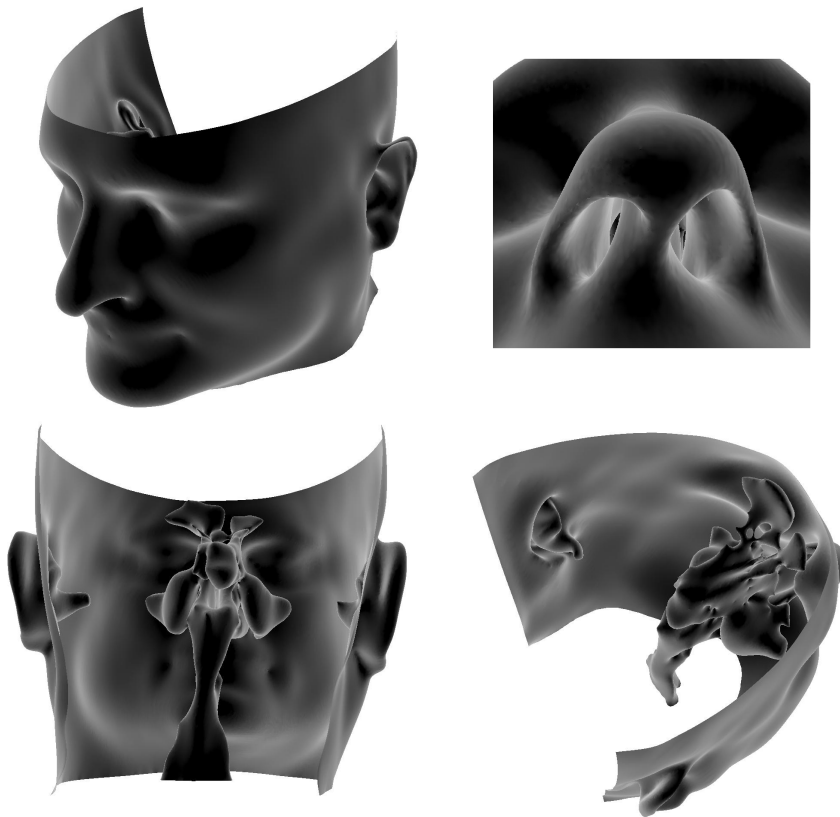


Fig. 5: The extracted inner and outer part of a human nose including the face is pictured in the images after the segmentation, surface reconstruction and smoothing process.

After the voxelization process, Γ_h is split in $k \in \mathbb{N}$ disjoint parts Γ_h^i , i.e. $\Gamma_h = \bigcup_{i=2}^{k+1} \Gamma_h^i$, which allows to handle different kinds of boundary conditions. Thereunto, *HyperMesh* offers a graphical user interface that allows an interactive manual marking of single voxels but also of sets of voxels.

In order to simplify the notation, the voxel mesh $\Omega_h \cup \Gamma_h$ is extended to a cuboid-shaped lattice $\tilde{\Omega}_h$ which can be identified by a d -dimensional matrix $\mathbf{A} \in \times_{j=1}^d \mathbb{N}^{n_j}$ where $n_j \in \mathbb{N}$ for $j = 1, 2, \dots, d$. Each voxel $\mathbf{r} \in \tilde{\Omega}_h$ is mapped to exactly one entry $\mathbf{A}(\mathbf{r})$ in \mathbf{A} . In the following, its value is said to be the *material number*. It is defined according to

$$\mathbf{A}(\mathbf{r}) := \begin{cases} 1 & : \text{ if } \mathbf{r} \subseteq \Omega_h \\ i & : \text{ if } \mathbf{r} \subseteq \Gamma_h^i \\ 0 & : \text{ otherwise .} \end{cases} \quad (3)$$

For the geometry of the nose cavity setting $h = 0.45$ mm, the voxelizing and marking process leads to a mesh with 1,393,304 voxels in total. The assigned material numbers as well as the corresponding numbers of voxels are listed in Table 1. In Figures 6 and 8 the obtained voxel mesh is visualized by means of its material numbers.

material number	description	number of voxels
0	no fluid	11,451,556
1	fluid	1,065,810
2	wall	325,887
3	nasopharynx	510
4	right nostril	425
5	left nostril	672

Table 1: Obtained numbers of voxels which are assigned to different material numbers for the lattice $\Omega_h \cup \Gamma_h$ with $h = 0.45$ mm when discretizing the considered human nasal cavity. The corresponding voxel mesh is shown in Figure 6 and Figure 8.

5 From Volume Mesh to Simulation

The realization of an automated assignment of boundary conditions to particular voxels of the geometry poses a challenge. This is because in the framework of LBM, boundary conditions must be defined on a mesoscopic base, i.e. the distribution function f_i has to be defined for all in the fluid pointing directions $v_i \in Q^{in}$. For the *bounce back* condition, which is imposed to realize a *no-slip*

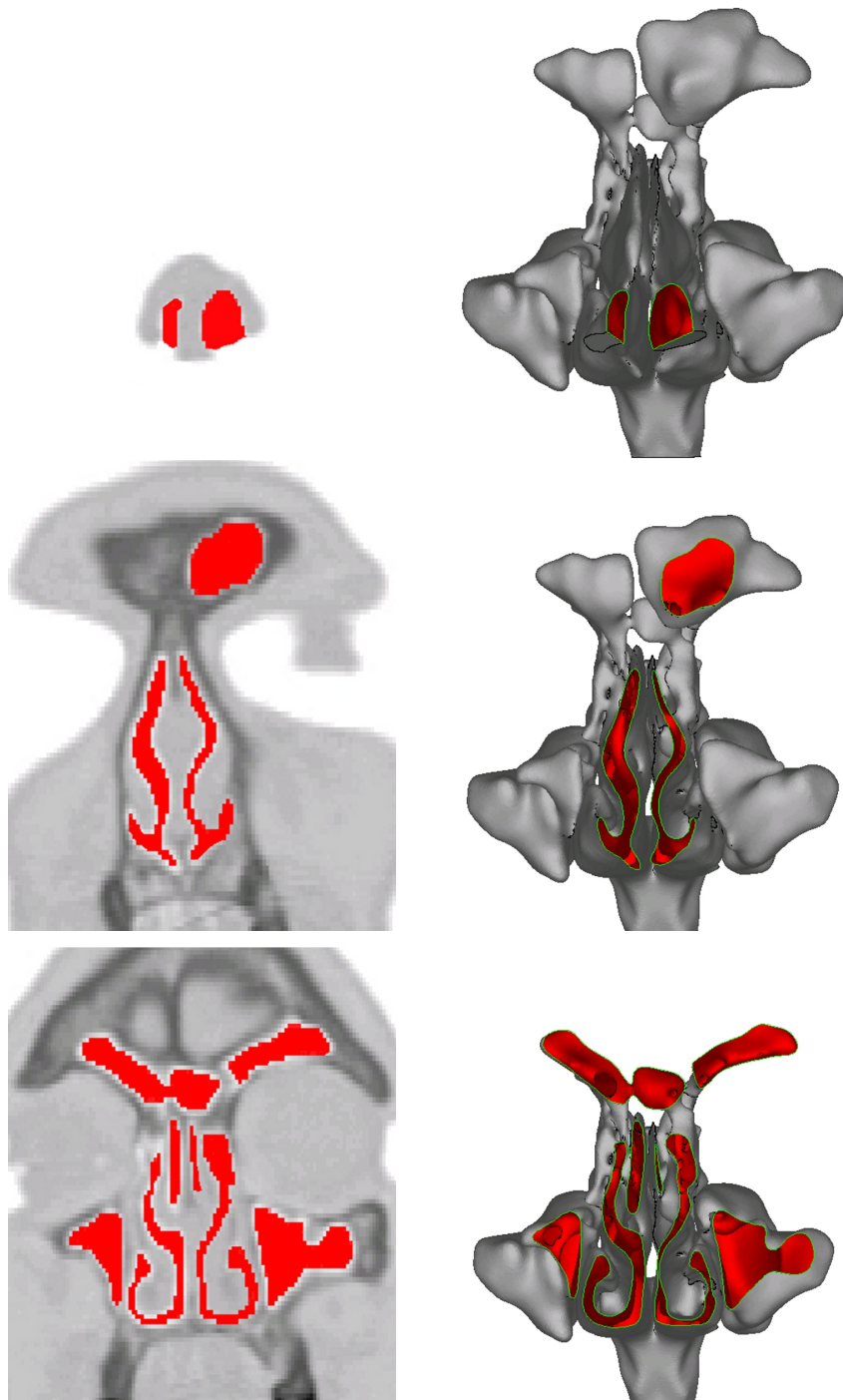


Fig. 6: Segmented CT data (left) and cross-section of the STL surface representation (right) both from top to bottom at $y = r_2 = 0.01, 0.04, 0.05$ m.

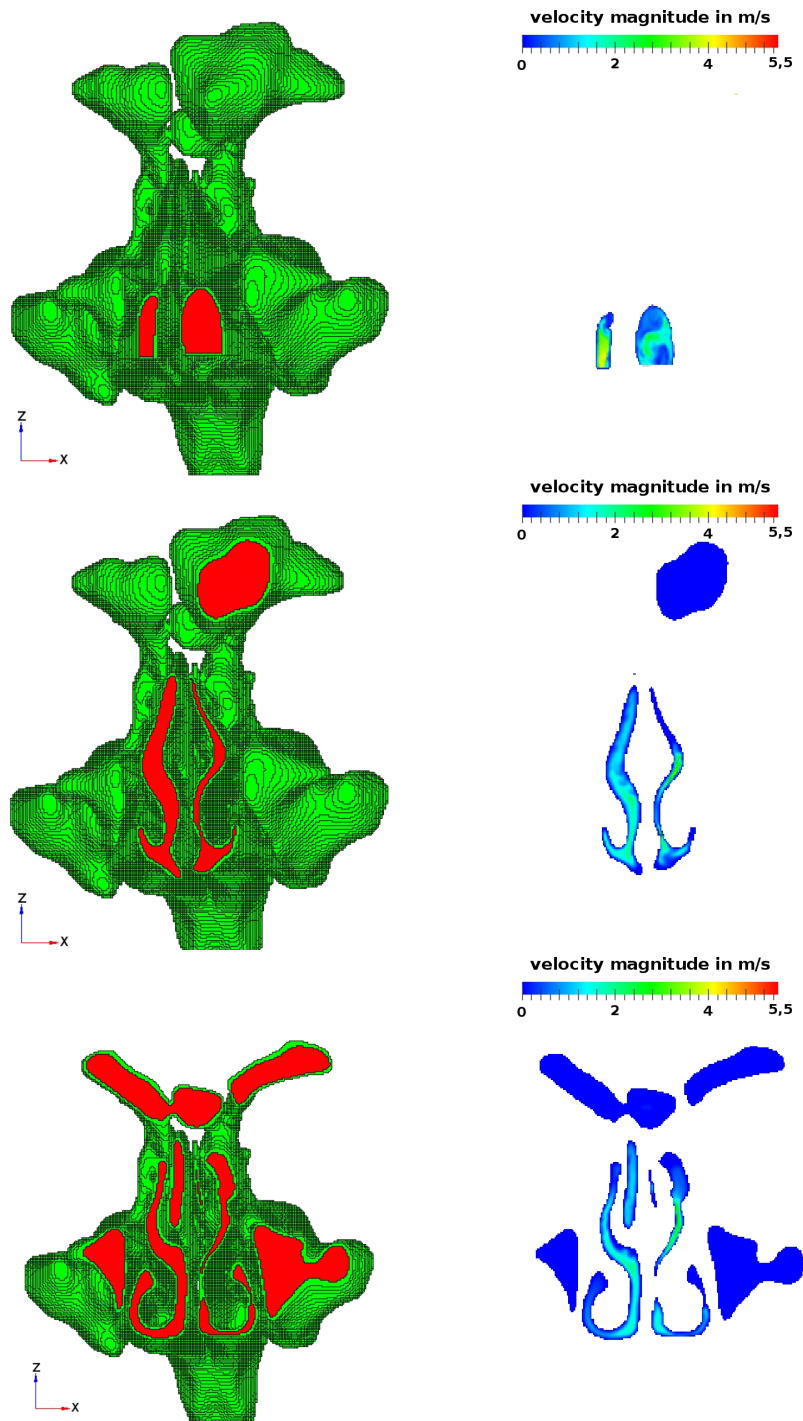


Fig. 7: Cross-section of the voxel mesh (left) and simulation results (right) obtained for a ventilation rate of 250 m/s both from top to bottom at $y = r_2 = 0.01, 0.04, 0.05$ m.

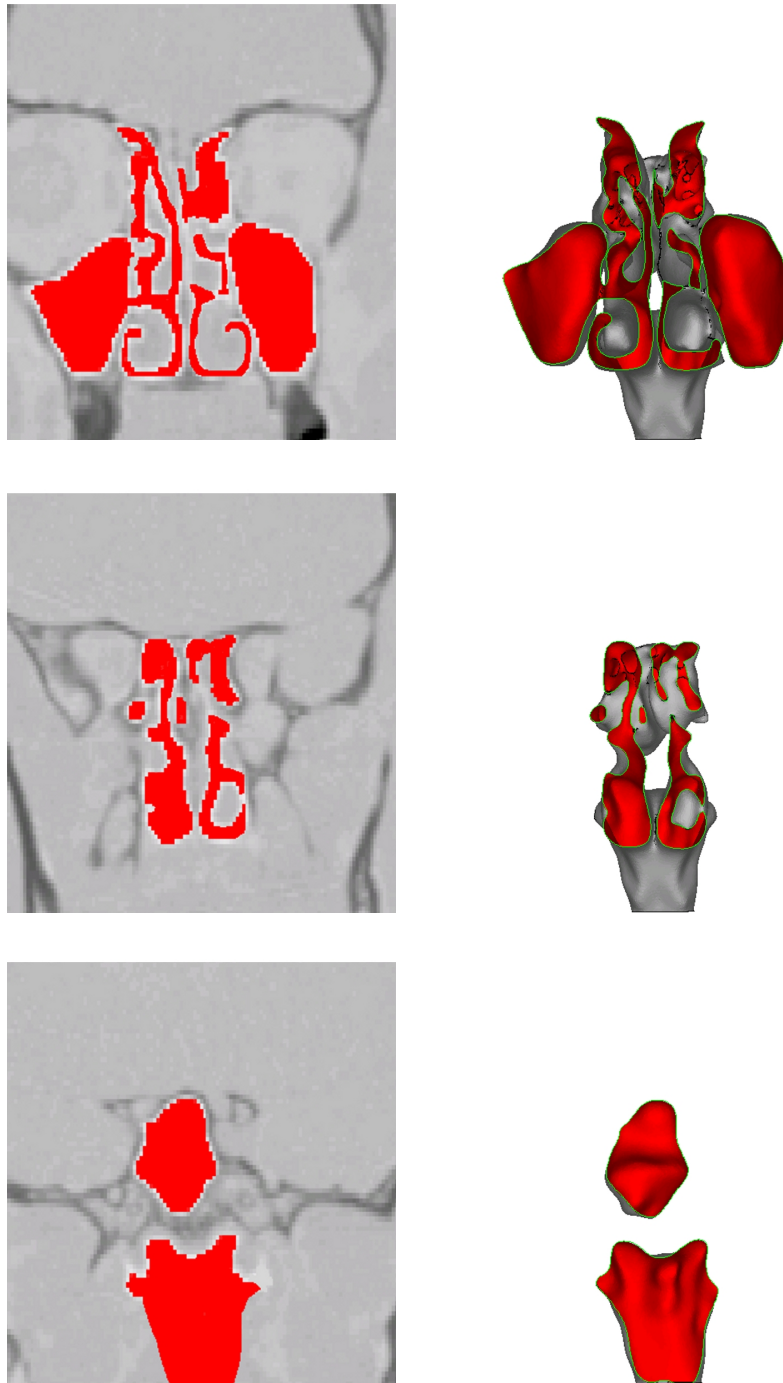


Fig. 8: Segmented CT data (left) and cross-section of the STL surface representation (right) both from top to bottom at $y = r_2 = 0.07, 0.09, 0.10$ m.

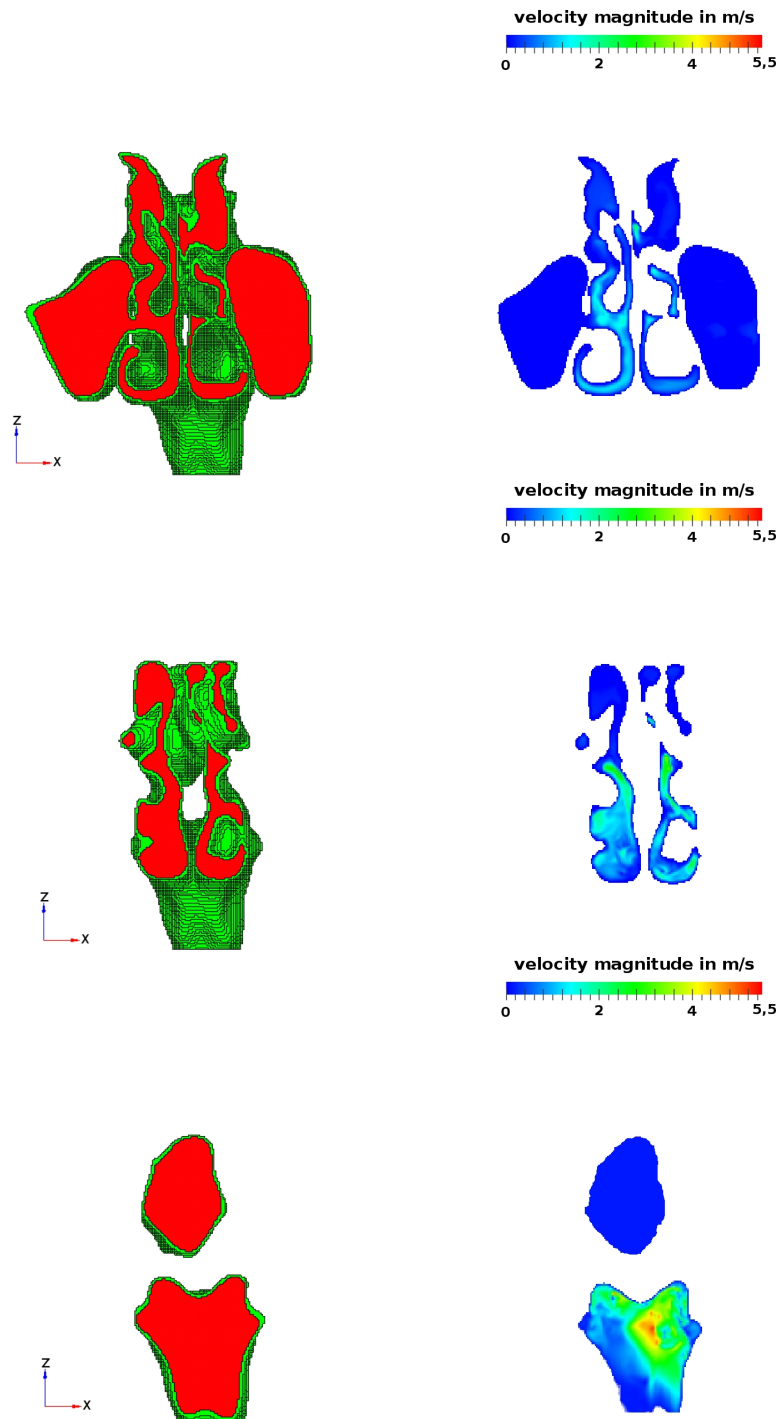


Fig. 9: Cross-section of the voxel mesh (left) and simulation results (right) obtained for a ventilation rate of 250 m/s both from top to bottom at $y = r_2 = 0.07, 0.09, 0.10$ m.

wall, this is not a problem. However, it is for the realization of inlet and outlet conditions where particular macroscopic moments are fixed. Here, the number of directions $v_i \in Q^{in}$, which point into the fluid, varies depending on the neighborhood of the considered node $\mathbf{r} \in \Gamma_h$. Frequently used approaches like those of Inamuro et al. [28], Skordos [49] or Latt [37,38] use finite differences to compute the wanted distributions f_i for $v_i \in Q^{in}$. Latt realizes the mentioned methods in the framework of OpenLB for 46 cases of possible neighborhoods for the 3D case, i.e. $d = 3$ (cf. OpenLB user guide associated with release 0.4 [36]). Yet, in practice this classification is not sufficient to handle all possible cases which emerge when considering complex geometries. Zimny faces this challenge in [56]. At first, the number of all possible cases is reduced by posing the following conditions, namely

1. Every single boundary voxel is at least neighbor of one fluid voxel.
2. Non of the fluid voxels is a neighbor of any non-fluid voxel.

Then, routines are realized which enable to modify the original voxel mesh matrix \mathbf{A} automatically such that theses two conditions hold. Additionally, with the help of a refinement algorithm the number of cases can be reduced to 96. The refinement scheme splits one voxel into N^d where $N \in \mathbb{N}$. In the following, N is called the *refinement level*. In accordance with the first of the two conditions, all not needed boundary voxels are removed. Further, Zimny succeeds in leading back the 96 cases to the 46 categories mentioned before. An automated assignment of one of the 46 categories to a boundary voxel is implemented and validated by comparing the results obtained for a benchmark problem, namely the flow around a circular cylinder, with those obtained by others which are summarized in the work of Schäfer et al. [45].

For the two considered geometries the mentioned techniques introduced and realized in OpenLB by Zimny are applied to automatize the initialization process. The macroscopic values imposed for the inlet and outlet conditions are provided by means of one function for each different boundary type $i = 2, 3, \dots$ of Γ_h^i .

6 Numerical Simulation and Postprocessing

In this section, numerical simulation results of respirations in a completely resolved nasal cavity are presented and discussed. The main aim of this study is to illustrate the application of the here presented preprocessing approach for a realistic complex problem. The study pays great attention to demonstrate the reliability of the presented approach. Therefore, several tests are performed to validate the obtained results. Furthermore, since the chosen underlying computational domain is obtained from a patient with a diagnosed pathology, emphasis in this study is placed on revealing possible abnormal specifics in the flow characteristics.

Flow characteristics in the human nose have already been studied both experimentally and numerically. Thereby, the focus is often placed on revealing the

morphological dependencies on the flow regime. For example, the experimental-based studies of Ploetz [43], Courtiss and Goldwyn [13], Scherer et al. [46] and Elad et al. [15] discuss controversially the role of the turbinates concerning laminarity and turbulence. Churchill et al. [12] also address this issue but vary other morphological parameters like the nostrils angle. Furthermore, this work is interesting because a detailed review about further investigations of morphological issues is provided. Numerical simulations of intranasal flows have been performed at least since 1995 (cf. Keyhani et al. [32]). Since then, correlated with the increase of computational power the underlying geometry and physical models have become more and more complex. In [29] for example, an overview of recently published articles in this context is provided. LBM are considered to face the problem by Freitas [18,19] and Finck et al. [16]. In contrast the approach presented here, in many studies the full complexity of the geometry, in particular the sinuses, is not mapped to the geometry model (cf. [16,18,19,27,29]). Moreover, convergence studies of the numerical simulations are hardly provided at all. In the remainder of this section other approaches are mentioned, whereby further distinctions are stressed.

The intranasal flows are simulated with the software *OpenLB* (cf. Appendix B). Advantage is taken of a hybrid parallelization concept which has been proposed by Krause et al. in [25] and is also part of the latest OpenLB release. Another open source software, namely *ParaView*, is employed for the visualization of the results, i.e. in particular the distributions of the flow fields in the nasal cavity. Like OpenLB, ParaView also runs in parallel on many platforms. It additionally offers 3D visualization from which permits a better understanding of the visualized velocity distribution in the complex shape of the nasal cavity.

6.1 Problem Formulation and Discretization Issues

The airflow in an inner human nose, which occurs during an expiration is to be simulated at different fixed flow rates, namely $Fl = 100$ ml/s, 125 ml/s, 167 ml/s, 250 ml/s and 333 ml/s. These rates are typically measured for male adults who rest, sit awake or do light exercises (cf. Valentin et al. [54]). In order to be able to well-define all problems, it is assumed that for each of the considered rates an unique *pseudo steady state* exists.

The underlying geometry $\Omega \cup \Gamma$ is extracted from CT scans of a 46 years old man as described in Section 3. For this patient Giotakis [8] diagnosed a *peripheral obstructive ventilation disorder*. The researched man is 1.98 m tall and weighs 105 kg.

The tests consider expirations with one inflow located at the boundary Γ^3 which is close to the nasopharynx and two outflows located at both nostrils, denoted by Γ^4 and Γ^5 . The rest of the boundary $\Gamma^2 = \Gamma \setminus (\Gamma^3 \cup \Gamma^4 \cup \Gamma^5)$ is assumed to be a wall with a no-slip property. The pressure at the nostrils Γ^4, Γ^5 is fixed to 1,013 hPa, and the temperature of the air is assumed to be $T = 20^\circ\text{C}$. Thus, the air is at standard conditions so that its speed of sound is $c_s = 343$ m/s, its density is $\rho = 1.225$ kg/m³ and its kinematic viscosity is $\nu = 1.4 \cdot 10^{-5}$ m²/s. The area of the boundary at the nasopharynx Γ^3 covers $A = 1,0328$ cm². With

it, the mean speed $U_{mean}(Fl)$ that is needed to reach the desired flow rates Fl can be computed. The characteristic macroscopic velocity is set to this mean speed $U_{mean}(Fl)$ and the characteristic macroscopic length is fixed to

$$L := \max_{r \in \Gamma^3} r_1 - \min_{r \in \Gamma^3} r_1 = 0.0162 \text{ m} .$$

Then, for each considered flow rate Fl the Reynolds number Re and the Mach number Ma can be computed. Table 2 shows the obtained characteristic quantities for different flow rates.

Fl	U_{mean}	Re	Ma
100 ml/s	0.97 m/s	1,120	0.0028
125 ml/s	1.21 m/s	1,401	0.0035
150 ml/s	1.45 m/s	1,681	0.0042
167 ml/s	1.62 m/s	1,871	0.0047
250 ml/s	2.42 m/s	2,801	0.0071
333 ml/s	3.22 m/s	3,731	0.0094

Table 2: Obtained characteristic speeds U_{mean} , Reynolds numbers Re and Mach numbers Ma for different flow rates Fl . The air is considered at normal conditions (1,013 hPa, 20 °C). Thus, the kinematic viscosity is $\nu = 1.4 \cdot 10^{-5} \text{ m}^2/\text{s}$ and the speed of sound is $c_s = 343 \text{ m/s}$. The characteristic length is defined by $L := \max_{r \in \Gamma^3} r_1 - \min_{r \in \Gamma^3} r_1 = 0.0162 \text{ m}$.

Due to the relative small occurring Mach numbers and the fact that under normal conditions air is a Newtonian fluid, the flow problems can be described mesoscopically with the BGK-Boltzmann equation as the governing equation and solved numerically with an LBM (cf. Section 2). A standard $D3Q19$ LB scheme is chosen to solve the problems. The uniform grid $\Omega_h \cup \Gamma_h$ with $\Gamma_h = \Gamma_h^2 \cup \Gamma_h^3 \cup \Gamma_h^4 \cup \Gamma_h^5$ is obtained as stated in Section 4 for several discretization parameters $h = 0.45 \text{ mm}/N$ where $N = 1, 2, 3$ denotes the discretization level.

The pressure and velocity boundary conditions are realized as proposed by Skordos [49]. A half-way *bounce back* condition is applied to approximate the no-slip property of the wall. For simplification, it is assumed that the velocity at the nasopharynx Γ_h^3 is distributed in the same way as in a pipe where Poiseuille's law holds. Thus, the velocity is a quadratic function of the distance from the center of the plane Γ_h^3 . The magnitude of the velocity distribution is increased linearly with the number of time steps up to 10,000 steps. Thereby, the slope is chosen so that the desired mean flow rate U_{mean} is reached at the time step 10,000. This start-up process aims to avoid unnatural behavior as well as numerical artefacts caused e.g. by a violation of smoothness. To reduce the total number of needed time steps to reach the pseudo steady states, the problems are considered after

a scaling. Thereto, the characteristic speeds and the kinematic viscosity are set to

$$\begin{aligned}\tilde{U}_{mean} &:= \frac{U_{LB}}{h} U_{mean} , \\ \tilde{\nu} &:= \frac{U_{LB}}{h} \nu\end{aligned}\quad (4)$$

for different so called *lattice speeds* $U_{LB} := 0.1, 0.05, 0.01$. With this, the Reynolds numbers stay the same while the new Mach numbers \widetilde{Ma} increase. The speed of sound in an LB simulation is set to $c_s = h^{-1}$. Thus, one obtains $\widetilde{Ma} = U_{LB} U_{mean}$ which is greater than the actual Mach number Ma in all considered cases. If one sets $Fl = 333$ ml/s, $\widetilde{Ma} < 0.3$ will hold for the lattice speeds $U_{LB} = 0.05, 0.01$. For simplification, the density $\rho = 1.225$ kg/m³ is scaled to the value of $\tilde{\rho} = 1$. The Maxwell distribution with $\mathbf{u} = \mathbf{0}$ and $\tilde{\rho} = 1$ in $\Omega_h \cup \Gamma_h$ serves as initial condition. The obtained results are finally rescaled to the original standard unit system.

6.2 Presentation and Discussion of the Numerical Results

All numerical results for the simulated expirations through both nostrils are obtained in parallel, either on the high performance computer *HP XC3000* at the *Karlsruhe Institute of Technology* (KIT) [2] or on the high performance computer *JUROPA* in Jülich [1]. Both, the full hybrid parallelization approach [25], which is realized using OpenMP and MPI in the framework of OpenLB, and its pure MPI-based part are employed. The hybrid parallel code related to the problem with $N = 2$, $U_{LB} = 0.05$ and $Fl = 125$ ml/s takes about four days to execute on the *HP XC3000* employing 128 cores in total on 32 nodes. The set-up time is included but for this example no output files for visualization are written. A detailed discussion of performance results for flow simulations in a human lung, obtained on *JUROPA* and also taking advantage of the hybrid parallelization approach [25], can be found in [34].

A quantity which is often used for validation (cf. e.g. [31,55,29]) is the total pressure drop as a function of the flow rate Fl

$$p_{\text{total}}(Fl) := p_{\text{nasopharynx}}(Fl) - p_{\text{nostrils}}(Fl) \quad (5)$$

occurring between the pressure at the inflow $p_{\text{nasopharynx}}$ and the outflows p_{nostrils} . The positions, where the values for the pressures are taken, are always set to be in the fluid close to the position in the centre of the area Γ_h^i , namely at

$$\mathbf{r}_{\text{mid}}^i := \frac{1}{2} \begin{pmatrix} \max_{\mathbf{r} \in \Gamma_h^i} r_1 + \min_{\mathbf{r} \in \Gamma_h^i} r_1 \\ \max_{\mathbf{r} \in \Gamma_h^i} r_2 + \min_{\mathbf{r} \in \Gamma_h^i} r_2 \\ \max_{\mathbf{r} \in \Gamma_h^i} r_3 + \min_{\mathbf{r} \in \Gamma_h^i} r_3 \end{pmatrix} - hN\mathbf{n} \quad (i = 3, 4, 5) . \quad (6)$$

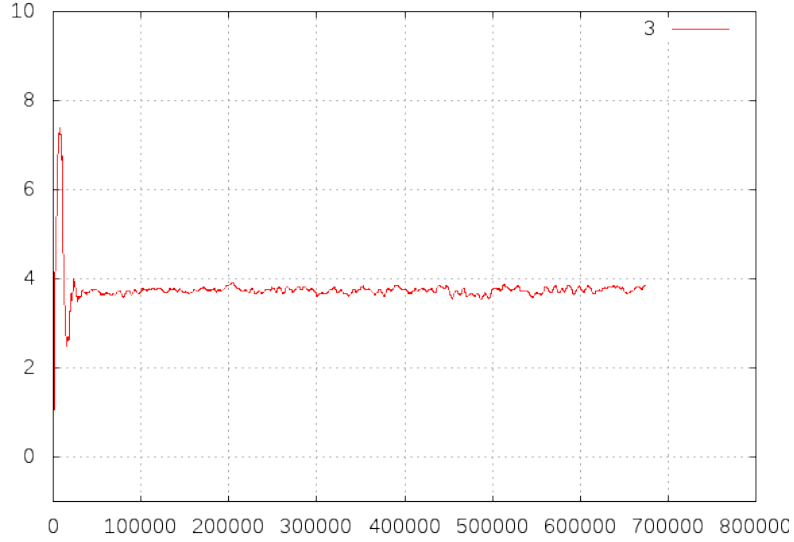


Fig. 10: Time evolution of the total pressure drop $p_{\text{total}}(Fl)$ at an expiration flow rate of $Fl = 125$ ml/s towards a pseudo steady state. The lattice speed is chosen to be $U_{LB} = 0.05$, and the refinement level is set to $N = 3$.

First, the convergence towards pseudo steady states for the simulated total pressure drops $p_{\text{total}}(Fl)$ is studied. Exemplarily, the case with an expiration flow rate of $Fl = 125$ ml/s is studied. For all other cases a similar behavior is observed. In Figure 10 the result for $p_{\text{total}}(Fl)$ is plotted as a function of time steps obtained for an LB simulation with a lattice speed of ($U_{LB} = 0.05$) based on a lattice which is refined with level $N = 3$.

The plot shows that after a certain number of time steps the quantity of interest oscillates in a certain range. This behavior is also observed for other choices of lattice speeds ($U_{LB} = 0.1, 0.05, 0.01$) and refinement levels ($N = 2, 3, 4$). Thereby, the frequency is found to be the smaller the greater the lattice speed is chosen. No significant differences are observed for the amplitude. The reasons for this noise might be related to the choice of the boundary condition at the outlet (see the discussion of artificial boundary conditions and especially *do-nothing* pressure boundary conditions for similar problems in Specovius-Neugebauer et al. [10,51]). In order to quantify the observations, the minimal $p_{\text{total}}^-(125)$ and maximal $p_{\text{total}}^+(125)$ computed values for the pressure drop, occurring between time step 400,000 and 600,000 are determined. Then, in order to obtain a basis for further comparisons, $\bar{p}_{\text{total}}(125)$ is set to the mean of the minimum and maximum. The quantitative results of the investigated case ($Fl = 125$ ml/s) are given in Table 3. They clearly show a satisfying convergence behavior. Hence the assumption of the existence of pseudo steady states is numerically evidenced.

N	U_{LB}	$p_{\text{total}}^+(125)$	$p_{\text{total}}^-(125)$	$\bar{p}_{\text{total}}(125)$
2	0.05	3.99	4.38	4.19
3	0.10	3.62	3.95	3.79
3	0.05	3.54	3.88	3.71
3	0.01	3.69	3.89	3.79
4	0.05	3.49	3.79	3.64

Table 3: Obtained results for the total pressure drop for different choices of lattice speeds U_{LB} and refinement levels N . $p_{\text{total}}^-(125)$ and $p_{\text{total}}^+(125)$ are the minimal and maximal computed values for the pressure drop occurring between time step 400,000 and 600,000 while $\bar{p}_{\text{total}}(125)$ denotes their mean.

Now, the numerical results are compared to those obtained by three other research groups. One result is obtained experimentally while the other two are obtained by numerical simulations with commercial CFD software. All three results are summarized in the graph in Figure 11.

The first of the three considered approaches is the experimentally obtained one. Kelly et al. [31] consider for their experiments a plastic replica of the nasal airways. Its underlying geometry is captured by means of MRI scans of a 53 year old male (cf. Swift [53]) without pathologies. The cast does not encompass all details of the human nose. In particular, the maxillary and frontal sinuses are not captured. However, the two airways up to the nasopharynx are considered in similar measures to those of the underlying geometry researched here.

The second data for comparison is computed numerically by Weinhold and Mlynski et al. [55]. The referred results are obtained for a 27 year old male with normal nasal anatomy. The computational domain is obtained by reconstructing a CT scan with a resolution of 1 mm to a 3D model where the sinuses are omitted. A finite volume scheme is employed to solve the incompressible Navier-Stokes equation together with a turbulence model of k - ϵ -type.

The last dataset is provided by Inthavong et al. [29], who consider a more complex physical model which in addition describes the heat transfer in the human nose. The underlying geometry is the nose of a 25 years old healthy Asian male, again, without the sinuses. The 3D model is constructed based on CT scans. For the computation of flow rates up to 250 ml/s a laminar, for high flow rates a turbulent k - ϵ -type model is employed.

All three cases differ to a greater or lesser extent to each other and also to the considered case in this paper. Distinctive features are e.g. their underlying geometries, the chosen physical models or the employed numerical methods. Disregarding these differences, all results for the pressure drops are found fairly close to each other. On the one hand can be concluded that the presented approach for the particular case is validated, on the other hand, in consideration of the mentioned differences, critical questions concerning the informative value of the computed total pressure drops arise. Further, for the considered patient a peripheral obstructive ventilation disorder is diagnosed (cf. Giotakis [8]). Yet, the

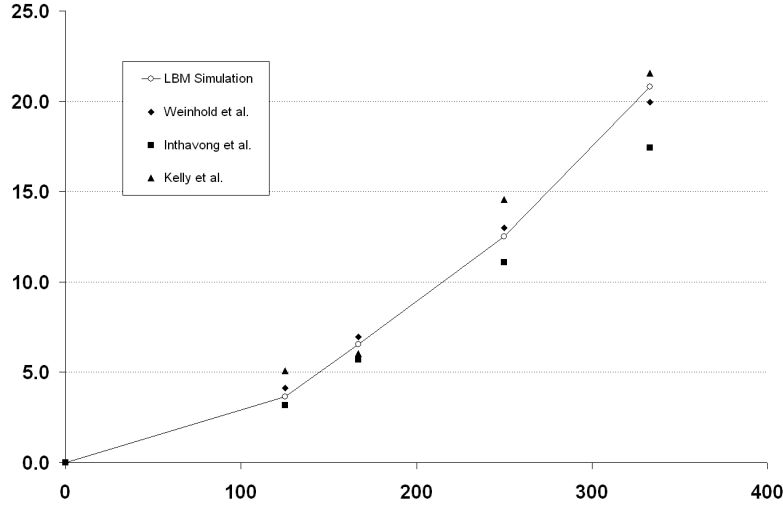


Fig. 11: Comparison between the numerical results for the pressure drop $\bar{p}_{\text{total}}(Fl)$ (Pa) for different flow rates Fl (ml/s) and the results obtained numerically by Weinhold et al. [55], Inthavong et al. [29] and experimentally by Kelly et al. [31].

results are found in good agreement to others which are based on data from patients who are classified to have no pathologies. This leads to the reasoning that the benefit of simulating the total pressure drop seems to be limited for medical applications. However, in [33] Krause considers respirations through only one nostril at a time. Thereby, the underlying geometry is exactly the same as the one considered here and also the problems are formulated analogously. Comparing the numerical results with measurements from the very patient obtained by rhinomanometry methods, Krause observes quantitative agreement.

The obtained velocity field for a flow rate of $Fl = 250$ ml/s is presented in the Figures 6 and 8 by means of a colored representation of the velocity magnitude in six chosen cross-sections. A 3D impression of the computed flow field is suggested through the pictures in Figure 12. There, the velocity magnitude is visualized by a number of colored 3D spheres for an expiration flow rate of $Fl = 100$ ml/s. Particularly important to note is the right upper picture which clearly displays high velocity magnitudes at the left inferior meatus. Indeed, a deeper analysis reveals that the highest values in the whole domain, namely about 1.64 m/s, are obtained there. Further, it is determined that only approximately 26 ml of the total 100 ml/s leave the left nostril. This asymmetrical behavior may be caused by a stenosis in that particular part of the geometry which is possibly the reason for the diagnosed peripheral obstructive ventilation disorder.

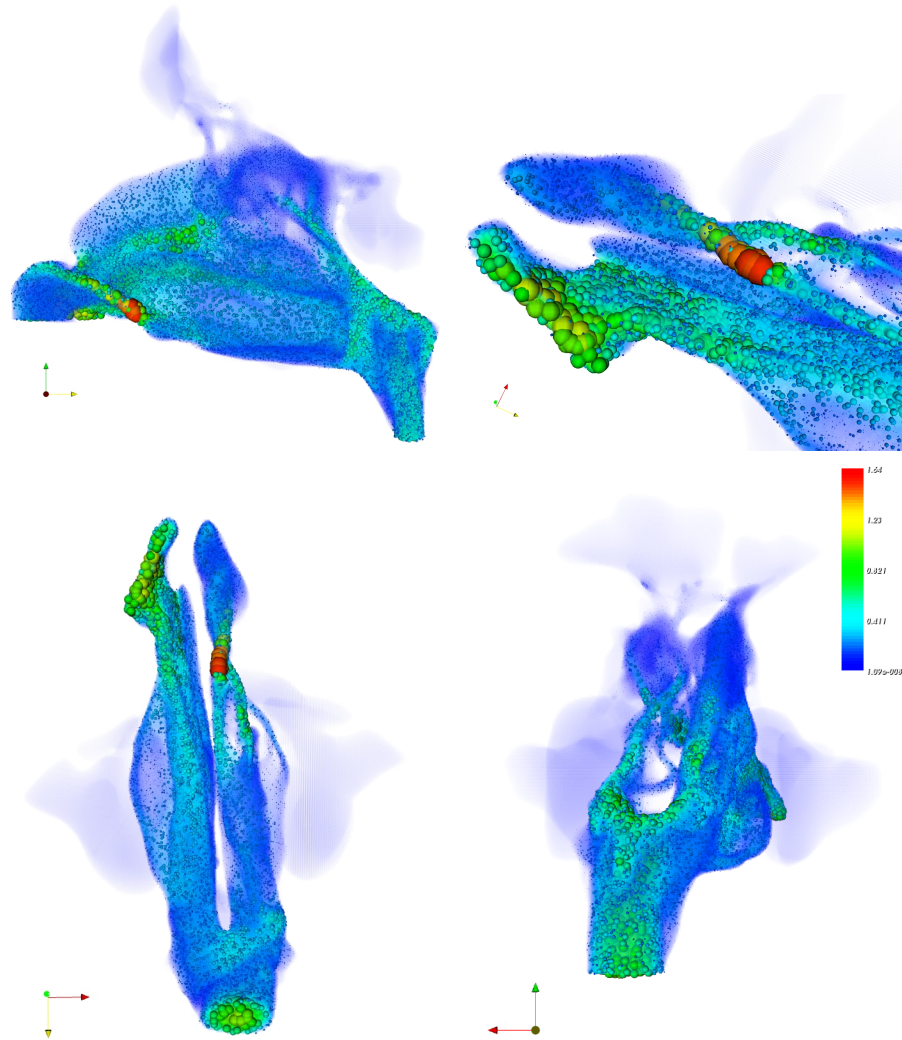


Fig. 12: The simulated flow field for an expiration flow rate of $Fl = 100$ ml/s is shown from different points of views, whereby the right upper picture displays a closer look to a significant narrow at the left inferior meatus. The magnitude of the velocity is visualised as coloured 3D spheres. The lattice speed in the LB simulation is set to $U_{LB} = 0.01$. No refinement is done ($N = 1$); and the simulation is stopped after 550,000 times steps have been performed.

Conclusion

The presented preprocessing approach is introduced as part of a concept dedicated for patient-specific full numerical simulations of respiratory flows. Advantage is taken by choosing LBM as discretization method since they are found to simplify the preprocessing substantially, yet achieving results as accurate as other numerical discretization methods have achieved for similar complex problems. This is shown by means of a case study, namely the full numerical simulation of an expiration through a human nasal cavity. The challenges concerning the preprocessing, which arise from the highly complex geometry that nowadays available CT scanners cannot capture exactly, is faced by taking advantage of Materialise's software packages Mimics and 3-matics. Here, especially the graphical user interface and many partly automated routines enable a qualitatively good segmentation and afterwards reconstruction of the complete nasal cavity from CT data. After applying a standard voxelization technique, an innovative strategy for an automated assignment of different boundary conditions dedicated for LBM is applied successfully the first time for a complex geometry. This completes the preprocessing process. The numerical simulations, performed afterwards, lead to results which are found to be independent of the mesh resolution. They are validated by comparing them with results obtained by others who applied fundamentally different discretization strategies. A located stenosis and other quantitative as well as qualitative results clearly show the great social impact and economic potential of the approach. Further automatization of the proposed preprocessing steps based on LBM will enable patient-specific simulations in future, which will lead to substantial improvements in the physicians' daily routines: stenoses and other causes of respiratory illnesses could be located or the achievable benefit of a surgery could be quantified beforehand.

Acknowledgments

The authors thank the group of Prof. Dr. Werner Heppt at the *Städtisches Klinikum Karlsruhe* that provided patient specific CT data and the Jülich Supercomputing Centre for providing the computing resources for the *HKA06* project.

References

1. *Juropa-JSC - HPC-FF*, August 2009.
2. *HP XC3000: Brief Information for new Users*, February 2010.
3. 3D Systems, Inc., 333 Three D Systems Circle Rock Hill, SC 29730 USA. *Stereolithography Interface Specification*, October 1989.
4. R. Adams and L. Bischof. Seeded Region Growing. *IEEE Trans. Pattern Anal. Mach. Intell.*, 16(6):641–647, 1994.
5. Mark Ainsworth and John Tinsley Oden. *A posteriori error estimation in finite element analysis*. Pure and applied mathematics, A Wiley-Interscience publication. Wiley, New York, 2000.

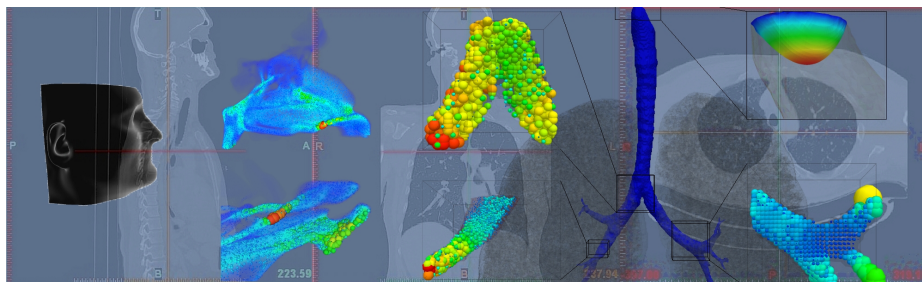
6. Altair Engineering Inc., 1820 E. Big Beaver Rd., Troy, MI 48083-2031 USA. *Altair HyperMesh: The Fastest, Solver Neutral CAE Environment for High Fidelity Modeling*, April 2010.
7. Lisa S. Avila, editor. *The VTK users guide : updated for VTK version 5*. Kitware, [New York], 2006. CD-ROM u.d.T.: The visualization toolkit, Version 5.0.4.
8. M. Baumann, E. Giotakis, W. Heppt, V. Heuveline, M.J. Krause, R. Mayer, and P. Weber. United Airways: Numerical Simulation of the Human Respiratory System, 2008. <http://www.united-airways.eu>.
9. Fokko Beekhof. CVMLCPP: Common Versatile Multi-purpose Library for C++, Web page. online, April 2010. <http://tech.unige.ch/cvmlcpp>.
10. S. Blazy, S. Nazarov, and M. Specovius-Neugebauer. Artificial Boundary Conditions of Pressure Type for Viscous Flows in a System of Pipes. *Journal of Mathematical Fluid Mechanics*, 9:1–33, 2007.
11. B. Chopard and M. Droz. *Cellular automata modeling of physical systems*. Cambridge University Press, 1998.
12. S.E. Churchill, L.L. Shackelford, J.N. Georgi, and M.T. Black. Morphological variation and airflow dynamics in the human nose. *Am. J. Hum. Biol.*, 16:625–638, 2004.
13. Eugene H. Courtiss and Robert M. Goldwyn. The Effects of Nasal Surgery on Airflow. *Plastic and Reconstructive Surgery*, 72(1):9–19, 1983.
14. Babuška, Ivo [Editor]. Modeling, mesh generation, and adaptive numerical methods for partial differential equations. Number 75 in The IMA volumes in mathematics and its applications, New York, 1995. Springer.
15. D. Elad, R. Liebenthal, B. L. Wenig, and S. Einav. Analysis of air flow patterns in the human nose. *Medical and Biological Engineering and Computing*, 31(6):585–592, 1993.
16. M. Finck, D. Hänel, and I. Wlokas. Simulation of nasal flow by lattice Boltzmann methods. *Comput. Biol. Med.*, 37(6):739–749, 2007.
17. Global Initiative for Asthma. Global Strategy for Asthma Management and Prevention. 2009.
18. Rainhill K. Freitas. *Lattice Boltzmann methods for internal flows*. PhD thesis, Aachen Technische Hochschule, 2008.
19. Rainhill K. Freitas and Wolfgang Schröder. Biofluidmechanik: Simulation der Luftströmung in den Atemwegen. 105(27):A–1512, 2008.
20. Thomas Gengenbach. Modellierung und numerische Simulation der menschlichen Atemwege auf Hochleistungsrechnern. Diplomarbeit, Universität Karlsruhe (TH), Fakultät für Mathematik, April 2009.
21. Thomas Gengenbach, Mathias J. Krause, and Vincent Heuveline. Numerical Simulation of the Human Lung: A Two-scale Approach. In Olaf Dössel, editor, *accepted for Biomedical Engineering*. De Gruyter, 2010.
22. Dieter Hänel. *Molekulare Gasdynamik*. Springer, 2004.
23. Robert M. Haralick and Linda G. Shapiro. Image segmentation techniques. *Computer Vision, Graphics, and Image Processing*, 29(1):100 – 132, 1985.
24. Xiaoyi He, Qisu Zou, Li-Shi Luo, and Micah Dembo. Analytic solutions of simple flows and analysis of nonslip boundary conditions for the lattice Boltzmann BGK model. *Journal of Statistical Physics*, 87(1):115–136, 1997.
25. V. Heuveline, M.J. Krause, and J. Latt. Towards a hybrid parallelization of lattice Boltzmann methods. *Computers & Mathematics with Applications*, 2009.
26. V. Heuveline and J. Latt. The OpenLB project: an open source and object oriented implementation of lattice Boltzmann methods. *Int. J. Mod. Phys. C*, 18:627–634, 2007.

27. I. Hörschler, Ch. Brücker, W. Schröder, and M. Meinke. Investigation of the impact of the geometry on the nose flow. *European Journal of Mechanics - B/Fluids*, 25(4):471 – 490, 2006.
28. Takaji Inamuro, Masato Yoshina, and Fumimaru Ogino. A non-slip boundary condition for lattice Boltzmann simulations. *Phys. Fluids*, 7:2928–2930, 1995.
29. K. Inthavong, J. Wen, J. Tu, and Z. Tian. From CT Scans to CFD Modelling - Fluid and Heat Transfer in a Realistic Human Nasal Cavity. *Engineering Applications of Computational Fluid Mechanics*, 3(3):321–335, 2009.
30. Michael Junk and Axel Klar. Discretizations for the Incompressible Navier-Stokes Equations Based on the Lattice Boltzmann Method. *SIAM J. Sci. Comput.*, 22(1):1–19, 2000.
31. J. T. Kelly, B. Asgharian, J. Kimbell, and B. Wong. Particle Deposition in Human Nasal Airway Replicas Manufactured by Different Methods. Part I: Inertial Regime Particles. *Aerosol Science and Technology*, 38(11):1063–1071, November 2004.
32. K. Keyhani, P. W. Scherer, and M. M. Mozell. Numerical Simulation of Airflow in the Human Nasal Cavity. *Journal of Biomechanical Engineering*, 117(4):429–441, 1995.
33. Mathias Joachim Krause. *Fluid Flow Simulation and Optimisation with Lattice Boltzmann Methods on High Performance Computers: Application to the Human Respiratory System*. PhD thesis, Karlsruhe Institute for Technology (KIT), Universität Karlsruhe (TH), Kaiserstraße 12, 76131 Karlsruhe, Germany, July 2010.
34. M.J. Krause, T. Gengenbach, and V. Heuveline. Hybrid Parallel Simulations of Fluid Flows in Complex Geometries: Application to the Human Lungs. In *accepted for Euro-Par 2010 Workshops*, 2010.
35. J. Latt. How to implement your DdQq dynamics with only q variables per node (instead of 2q). Technical report, Tufts University Medford, USA, 2007.
36. J. Latt. *OpenLB User Guide Associated to Release 0.4 of the Code*. OpenLB, 2008.
37. Jonas Latt. *Hydrodynamic limit of lattice Boltzmann equations*. PhD thesis, University of Geneva, Geneva, Switzerland, 2007.
38. Jonas Latt and Bastien Chopard. Lattice Boltzmann Method with regularized non-equilibrium distribution functions. *Math. Comp. Sim.*, 72:165–168, 2006.
39. Jonas Latt, Bastien Chopard, Orestis Malaspinas, Michel Deville, and Andreas Michler. Straight velocity boundaries in the lattice Boltzmann method. *Phys. Rev. E*, 77:056703, 2008.
40. Medical Imaging & Technology Alliance. *Digital Imaging and Communications in Medicine (DICOM), Part 1: Introduction and Overview*. National Electrical Manufacturers Association, 1300 N. 17th Street, Rosslyn, Virginia 22209 USA, 2009.
41. Fakir S. Nooruddin and Greg Turk. Simplification and Repair of Polygonal Models Using Volumetric Techniques. *IEEE Transactions on Visualization and Computer Graphics*, 9(2):191–205, 2003.
42. Materialise NV. Mimics Software: The standard in 3D image processing and editing based on CT or MRI data. <http://www.materialise.com/mimics>.
43. A. W. Proetz. Air currents in the upper respiratory tract and their clinical importance. *Ann Otol Rhino Laryngol*, 60:439–467, 1951.
44. Laure Saint-Raymond. From the BGK model to the Navier-Stokes equations. *Annales Scientifiques de l'École Normale Supérieure*, 36(2):271 – 317, 2003.
45. M. Schäfer and S. Turek. Benchmark Computations of Laminar Flow Around a Cylinder. Preprint 96-03, University Heidelberg, 1996.
46. P. W. Scherer, I. I. Hahn, and M. M. Mozell. The biophysics of nasal airflow. *Otolaryngologic Clinics of North America*, 22(2):265–78, 1989.

47. Tim Schröder. SOMATOM Sensation 64 - der schnellste Computertomograph der Welt. In *MEDICAL SOLUTIONS, Changing the Way Healthcare is Delivered*, pages 10–13. Siemens AG, November 2004.
48. Andreas Siebert. Dynamic Region Growing. In *Vision Interface*, 1997.
49. P. Skordos. Initial and boundary conditions for the Lattice Boltzmann Method. *Phys. Rev. E*, 48(6)(6):4823–4842, 1993.
50. British Thoracic Society. The Burden of Lung Disease. 2006.
51. Maria Specovius-Neugebauer. Approximation of the stokes Dirichlet problem in domains with cylindrical outlets. *SIAM J. Math. Anal.*, 30(3):645–677, 1999.
52. M. C. Sukop and D. T. Thorne. *Lattice Boltzmann modeling*. Springer, 2006.
53. D.L. Swift. Inspiratory Inertial Deposition of Aerosols in Human Nasal Airway Replicate Casts: Implication for the Proposed NCRP Lung Model. *Radiation Protection Dosimetry*, 38(1-3):29–34, 1991.
54. J. Valentin. Basic anatomical and physiological data for use in radiological protection: reference values - ICRP Publication 89. *Annals of the ICRP*, 32:1–277(277), September 2002.
55. Ivo Weinhold and Gunter Mlynski. Numerical simulation of airflow in the human nose. *European Archives of Oto-Rhino-Laryngology*, 261(8):452–455, 2004.
56. Simon Zimny. Numerische Simulation von intranasalen Strömungen mit Lattice-Boltzmann-Methoden. Diplomarbeit, Karlsruhe Institute of Technology (KIT), Universität Karlsruhe (TH), Fakultät für Mathematik, April 2010.

A The United Airways Project

The *United Airways*¹ project originates to cover numerical simulations in the whole human respiratory system, coupling nasal and oral airways, paranasal sinuses, pharynx, larynx, trachea, bronchioles and the respiratory zone. It is an interdisciplinary research project between mathematics, especially in the field of numerical simulations, modeling and optimization, medicine, otolaryngology and pulmonology in particular, engineering and computer science.



United Airways follows an integrative approach allowing for highly efficient airflow and particle flow simulations on high performance computers, using patient specific CT/MRT data as well as mathematical, statistical and probabilistic models for the respiratory system.

¹ <http://www.united-airways.eu>

The research focus on applications in public health lies on airflow and particle deposition patterns in the human respiratory system. Studies for early diagnosis and ease of pathologies through clinical surgery, rhinomanometrically validated flow simulations and optimizations of the efficacy of drugs administered through the airway system are carried out. To put this into practice, the project has to take the challenge in various research fields like dedicated modeling, optimization, automated preprocessing, efficient high performance computing and visualization.

The United Airways project follows two different methods to simulate the air-flow in the human respiratory system numerically. The first approach uses *finite elements methods* (FEM) to discretize the Navier-Stokes equation that models the fluid flow in a macroscopic fashion. The FEM methods are implemented in the framework of the software project *HiFlow3*². The second approach is based on lattice Boltzmann methods (LBM) and implemented in the *OpenLB* open source software package (cf. Appendix B). The fluid dynamics are described in terms of a mesoscopic model governed by the BGK-Boltzmann equation. Both strategies are well-suited for numerical simulations on high-performance computers and capable of computations on large and very complex geometries, arising from biological structures.

Publications related to the United Airways project cover preprocessing techniques [20,56], different models for the lower lungs [20,21] including parallel implementation and performance results, and numerical fluid flow simulations in the human lungs and the nose [20,33,34].

The United Airways project has been awarded in the contests *Itanium Innovation Awards* 2007 and 2009. The awards are given by the *Itanium Solutions Alliance* in four different categories for approaches of all areas of industry and research developed using *Intel Itanium*-based solutions. In both years, work related to the United Airways project has been submitted in the category *Humanitarian Impact*. The 2007 proposal has been awarded as *Finalist* together with others handed in by applicants of e.g. the Stanford University and the Imperial College London. In 2009, the presented work has earned the title *Honorable Mention Finalist*.

B The OpenLB Project

The *OpenLB* project aims at setting up an open source implementation of *lattice Boltzmann methods* (LBM) in an object oriented framework. The code is written in C++ and intended to be used both by application programmers and by developers who may add their own particular dynamics. It supports advanced data structure that take into account complex geometries and parallel program executions.



² <http://www.hiflow3.org>

The programming concepts strongly rely on dynamic genericity via the use of object oriented interfaces as well as static genericity by means of templates. This design allows an efficient, straightforward and intuitive implementation of LBM. It is cross-verified for software quality by several reviewers and is presented along with a user guide. To the knowledge of the authors, the OpenLB project is the first attempt to produce a generic platform for LB programming and to share it with the community via a system of open source contributions.

An overview of the computational framework employed in OpenLB and the features of the latest release 0.5 of OpenLB is given in the following:

– **Overview Computational Framework:**

- Platform independent developments
- Modular, extensible C++ code
- Object-oriented programming style
- Template-based genericity
- Open source (GNU General Public License, version 2)

– **Overview Features:**

- 2D and 3D simulations by means of LBM
- Various LBM, e.g. BGK, MRT, Regularized LB [37,38]
- Various lattice types, e.g. $D2Q9$, $D3Q15$, $D3Q19$, $D3Q27$
- Multi physical models (multiphase, thermal flows)
- Local and non-local boundary condition types, e.g. Inamuro [28], He and Zou [24], Latt (regularized LB) [37,38]
- Checkpointing for interrupted program executions
- Parallelism for shared and distributed memory platforms
- Visualisation, e.g. based on VTK [7]
- Straightforward coupling to external tools for pre- and postprocessing

Furthermore, a documentation for developers as well as user guides for several releases are provided on the OpenLB website <http://www.openlb.org>. Beside the overview and technical reports, e.g. [35], given on the OpenLB website, one finds more details, in particular concerning the computational concepts realized in the OpenLB code, in [26]. Ongoing work concerning the hybrid parallelization strategy which has been realized in OpenLB is presented [25]. Latt, Malaspina et al. dedicate their work [39] to a comparison of various different approaches for LB-specific boundary conditions. The presented tests are performed using the OpenLB library.

OpenLB has played a major role in the two proposals of the *United Airways* project (cf. Appendix A) for the *Itanium Innovation Awards*. The contest is organized by the *Itanium Solutions Alliance* which is a global consortium of notable hardware, operating system and application vendors. Both presented solution strategies for numerical simulations of human respiratory flows were awarded in the category of *Humanitarian Impact* as *Finalist* in 2007 and as *Honorable Mention Finalist* in 2009.